PAPER

Improved capacitive deionization performance of mixed hydrophobic/hydrophilic activated carbon electrodes

IOP Publishing Journal of Physics: Condensed Matter
J. Phys.: Condens. Matter **28** (2016) 114003 (11pp) doi:10.1088/0953-8984/28/11/114003

Improved capacitive deionization performance of mixed hydrophobic/hydrophilic activated carbon electrodes

M Aslan[1], M Zeiger[1,2], N Jäckel[1,2], I Grobelsek[1], D Weingarth[1] and V Presser[1,2]

[1] INM-Leibniz Institute for New Materials, Campus D2 2, 66123 Saarbrücken, Germany
[2] Department of Materials Science and Engineering, Saarland University, Campus D2 2, 66123 Saarbrücken, Germany

E-mail: volker.presser@leibniz-inm.de

Received 29 June 2015, revised 20 October 2015
Accepted for publication 23 October 2015
Published 23 February 2016

Abstract

Capacitive deionization (CDI) is a promising salt removal technology with high energy efficiency when applied to low molar concentration aqueous electrolytes. As an interfacial process, ion electrosorption during CDI operation is sensitive to the pore structure and the total pore volume of carbon electrodes limits the maximum salt adsorption capacity (SAC). Thus, activation of carbons as a widely used method to enhance the porosity of a material should also be highly attractive for improving SAC values. In our study, we use easy-to-scale and facile-to-apply CO_2-activation at temperatures between 950 °C and 1020 °C to increase the porosity of commercially available activated carbon. While the pore volume and surface area can be significantly increased up to 1.51 cm^3 g^{-1} and 2113 m^2 g^{-1}, this comes at the expense of making the carbon more hydrophobic. We present a novel strategy to capitalize on the improved pore structure by admixing as received (more hydrophilic) carbon with CO_2-treated (more hydrophobic) carbon for CDI electrodes without using membranes. This translates into an enhanced charge storage ability in high and low molar concentrations (1 M and 5 mM NaCl) and significantly improved CDI performance (at 5 mM NaCl). In particular, we obtain stable CDI performance at 0.86 charge efficiency with 13.1 mg g^{-1} SAC for an optimized 2:1 mixture (by mass).

Keywords: capacitive deionization, wetting behavior, water desalination, porous carbon, physical activation

(Some figures may appear in colour only in the online journal)

1. Introduction

Capacitive deionization (CDI) is an emerging technology showing great promise for energy efficient desalination of saline water of low ionic strength [33, 40, 47]. The technology is based on reversible ion electrosorption in an electrical double-layer at the fluid – solid interface of saline solutions with electrified carbon [3]. Saline water streams are introduced to a CDI cell either by flowing parallel to (flow-by geometry) [14, 35] or vertically through [1, 46] porous electrodes. Conventional CDI operation is accomplished by cycling between ion removal and electrode regeneration modes, in which salt ions are electrosorbed from the inlet water stream or released back in the outflow stream. Continuous operation can be accomplished by replacing conventional film electrodes with flowable carbon suspensions, while maintaining the high charge efficiency (up to 95%) of CDI [22, 25].

Carbon materials are excellent electrode materials for CDI applications because many of them are derived from sustainable biomass, the synthesis costs are commonly very low, and

they possess the unique ability to realize high surface areas and precise matching of optimized pore size distribution [28]. Currently, the most promising materials for high CDI performance metrics (i.e., salt sorption capacity, SAC) are materials with a high surface area, such as activated carbons [37], carbide-derived carbons [39] and graphene-like materials [50]. Although the correlation is not linear, there is still a clear dependency between pore volume and SAC, and predictive tools to calculate the CDI performance of a material based on its porosity parameters have been devised [37].

Activation of carbons can be accomplished by chemical treatment in either reactive liquids (like molten KOH) or oxidative gaseous environments (such as water vapor or synthetic air) [29]. This paper addresses the effect of CO_2-activation of activated carbons (i.e., physical activation). Our choice of physical activation was motivated by the facile implementation even for large-scale synthesis; in contrast, the commonly employed KOH (chemical) activation requires thorough rinsing of the activated carbon material at the expense of an additional treatment step. In addition, CO_2-activation is a well-established process and has been shown in the field of supercapacitors to greatly enhance the electrochemical performance [8]. Also, improved CDI performance after physical activation has been reported for carbon fibers [13] or carbon aerogels [8].

The improved electrochemical performance after activation commonly correlates with the larger pore volume [23]. While the correlation between pore volume (or surface area) and electrochemical performance is neither linear nor straightforward [2, 7], there is still a strong agreement in the supercapacitor and CDI communities that a higher level of pore development is beneficial [31, 41, 43]. Motivated by work on aqueous and organic supercapacitors [9, 42], we have established recently a comprehensive model to correlate the pore structure with the CDI performance [37]. In short, the entire volume of micro- and mesopores is important to consider when attempting to predict the CDI performance, but the differential SAC (mg salt removed per cm^3 of incremental pore volume) is strongly enhanced for micropores [37]. This predictive model was corroborated by a recent study on heteroatom carbons, but an increased deviation between measured and calculated SAC was observed for a high content of electrochemically active non-carbon atoms [38].

Based on the current literature, it has been shown that CO_2-activation can be used to increase the pore volume, while the pore size distribution is only slightly modified [8]. We also know that a higher pore volume level may enhance the CDI performance. So far, no systematic study on this aspect has been carried out on high surface area activated carbon in consideration of the possible interplay of wettability and CDI charge efficiency. In our study, we provide data to show the potentials and limitations of CO_2-activation for improved CDI performances. We also introduce, by mixing hydrophobic and hydrophilic carbon, a novel strategy to exploit an improved porosity without sacrificing CDI salt removal capacity and efficiency in view of limited carbon wetting by aqueous media. This approach aligns with recent reports on the benefits of mixed hydrophilic materials for fluid transport [52].

2. Experimental description

2.1. Materials and carbon activation

Commercially available activated carbon (AC) named YP80 was purchased from Kuraray (Japan). Samples labeled 'as received' were used as received without any chemical or physical treatment of the material.

Physical activation in flowing CO_2 was carried out in a rotary quartz-glass tube furnace capable of treating 60 g AC powder per one run. The samples were heated at 10 °C min^{-1} to the activation temperature in flowing CO_2. After reaching the activation temperature (950, 970, 980, 1000, or 1020 °C), the temperature was held within ±1 °C for 2 h with a CO_2 gas flow of 80 $L/h = 1333$ sccm. Afterwards, the samples were cooled to room temperature in flowing CO_2 at 10 °C min^{-1}. CO_2-treated samples are named 'CO_2' and the superscript number (e.g., $CO_2^{980\ °C}$) indicates the activation temperature (duration of 2 h in all cases). Mixing of as received and activated material was accomplished by thorough homogenization by tumbling in a plastic jar with 10 mm plastic balls for 3 h.

2.2. Electrode fabrication

Film electrodes were prepared by mixing porous carbon material and polytetrafluoroethylene binder (PTFE, 60 mass% solution in water from Sigma Aldrich, USA) and ethanol to obtain homogeneous carbon paste. The carbon-to-binder mass ratio was 95:5. Afterwards, the carbon paste was rolled (MTI HR01, MIT Corp.) to 150 ± 20 mm thick free standing electrode films which were dried in an air atmosphere at 120 °C for 24 h at 20 mbar. For the CDI experiments the carbon electrodes were cut into square pieces of 6 × 6 cm^2 with a hole in the middle of each electrode of 1.5 × 1.5 cm^2. The final electrode mass density was 0.3–0.4 g cm^{-3} and the total electrode mass (for all six electrodes) was 1.4–1.6 g.

2.3. Structural and chemical characterization

Scanning electron microscope (SEM) images were collected with a JEOL JSM 7500F field emission scanning electron microscope (FESEM, Japan) operating at 3 kV. Energy dispersive x-ray spectroscopy (EDX) was carried out at the JEOL system with an X-Max Silicon Detector of Oxford Instruments using AZtec software (United Kingdom).

Raman spectra were measured with a Renishaw inVia Raman microscope (UK) using an Nd-YAG laser with an excitation wavelength of 532 nm (grating with 2400 lines mm^{-1}, spectral resolution of ~1.2 cm^{-1}, spot size on the sample in the focal plane ~2 μm, output power of 0.2 mW). Spectra were recorded for 20 s and accumulated 50 times to obtain a high signal-to-noise and signal-to-background ratio. Peak fitting was performed by employing four Lorentzian peaks for the spectrum between 900 cm^{-1} and 1900 cm^{-1}.

Specific surface area (SSA), pore volume and pore size distribution of the samples were measured by nitrogen gas sorption measurements at −196 °C with an Autosorb system (Autosorb 6B, Quantachrome) in the relative pressure range

from 0.008 to 1.0. Before the measurements, the powder samples were outgassed at 250 °C for 10 h under vacuum conditions at 10^2 Pa to remove adsorbed water; the outgassing temperature for film electrodes was 120 °C. Nitrogen gas sorption was performed in liquid nitrogen at −196 °C. The SSA was calculated with the ASiQwin-software using the Brunauer–Emmett–Teller (BET) [6] equation in the linear relative pressure range 0.01–0.05. We also calculated the SSA and pore size distribution (PSD) via quenched-solid density functional theory (QSDFT) [21] with a hybrid model for slit and cylindrical pores and pore size between 0.61 nm and 34 nm. The hybrid model yielded a better fit compared to a simple slit-shaped pore model.

Skeletal density of the samples was measured by helium gas pycnometer (AccuPyc 1330, Micromeritics).

Contact angle measurements of carbon film electrodes with demineralized water were carried out in air using an OC 25 system from DataPhysics (Germany). The contact angles were monitored over time, covering a range between 0.2 and 1000 s. The obtained data was smoothed over 10 data points on the time-axis.

Water vapor sorption was monitored as a function of exposure time by placing the samples in an air-tight container held at 75% relative humidity. The water vapor uptake was monitored by periodic mass measurements with a Sartorius microbalance (Germany) with an accuracy better than 1 μg.

Streaming potential measurements were conducted with a 100 mg carbon powder in 30 ml demineralized water after 10 min of ultrasound treatment and shaking for 10 h (Mütek PCD.03 pH, BTG Instruments, Germany). The initial pH value was adjusted at 9 with dosing ammonia solution, NH_4OH. Hydrochloric acid, HCl, was used as titrant down to pH 3.

2.4. Electrochemical and CDI testing

Prior to electrochemical testing, a 3 h resting period was maintained to ensure the removal of dissolved oxygen from the electrolyte via nitrogen gas bubbling and to achieve soaking of the electrodes. Electrochemical characterization of all the samples was carried out using a VSP300 potentiostat/galvanostat from Bio-Logic (France) operating in cyclic voltammetry (CV) or galvanostatic cycling (GC) mode. Specific capacitance, normalized to the performance of one electrode (as common in supercapacitor systems; [45, 53]) was calculated from the discharge current during galvanostatic discharging at different current densities (ranging from 0.1 to 10 A g^{-1}) after correcting for the iR drop.

For the desalination experiments a CDI device with flow-by mode was used which is described in [38]. The CDI stack was built from graphite current collectors (SGL Technologies, Germany; thickness: 250 μm) with attached porous carbon electrodes and a porous spacer (glass fiber pre-filter, Millipore, compressed thickness of a single layer: 380 μm). Each current collector was used for two adjacent cells, except for the bottom and the top which was only in contact with one carbon electrode. After stack assembly, the stack with two parallel flow paths was pressed together firmly and sealed. A constant flow rate of 7.5 ml min^{-1} per one flow channel was used. Ion adsorption and desorption steps are carried out using constant potential mode at 1.2 V. The electrode regeneration was accomplished at 0 V. For all electrochemical operations, we used a VSP300 potentiostat/galvanostat (Bio-Logic, France) and the duration of each half-cycle was 30 min. All experiments were carried out with 5 mM NaCl solution and a 10 L electrolyte vessel which was flushed continuously with N_2 gas to purge the water from dissolved oxygen. The salt adsorption capacity and the measured charge were defined per mass of total electrode material (AC + binder) in both electrodes and were calculated as an average value from the adsorption and desorption step. For calculation of the electrical charge, the leakage current measured at the end of each half-cycle was subtracted. Repeat experiments showed a reproducibility of the data of 5–10%.

3. Results and discussion

3.1. Structural and chemical carbon properties

The AC powder consisted of anisometric particles ranging from ca. 0.5 μm to 10 μm with an average aggregate size of around 2–5 μm (figures 1(A) and (B)) [24]. Locally, macropores (pores larger than 50 nm) can be seen with high resolution scanning electron microscopy (SEM; insets in figures 1(A) and (B)), but no significant change in morphology and texture was seen when comparing as received (figure 1(A)) with activated samples (e.g., $CO_2{}^{1020}$: figure 1(B)).

The CO_2-activation process only marginally impacts on the carbon structure (figures 1(C) and (D)). The Raman spectra of the samples show D- and G-modes between 1200 cm^{-1} and 1700 cm^{-1} characteristic for incompletely graphitized carbon, the corresponding overtones and the combinational modes between 2300 cm^{-1} and 3400 cm^{-1} (figure 1(C)). The G-mode at ca. 1600 cm^{-1} is a first-order peak with E_{2g}-symmetry and representative for sp^2-hybridized carbon [15]. The D-mode at ca. 1340 cm^{-1} relates to defects and disorder induced phonon transitions [36, 49]. For all samples, the full-width at half-maximum (FWHM) for the D- and G-modes varies marginally, ranging from 100.1 cm^{-1} to 105.9 cm^{-1} and 51 cm^{-1} to 55 cm^{-1}, respectively. Compared to the as received state, physical activation increases the integral peak ratio I_D/I_G (figure 1(D)), which can be seen as an indicator of structural disorder or the degree of graphitization [56]. An increased I_D/I_G ratio is indicative of a decrease in the carbon domain size and aligns well with the physical removal of material during activation. A subsequent decrease in I_D/I_G for higher activation temperatures illustrates the competing processes of activation (decrease in domain size) and enhanced carbon ordering (graphitization at higher temperatures). The overall increase, however, is small compared to the as received state and the carbon remains in an incompletely graphitized state.

While the morphology and the structure of the activated carbon material remain largely unchanged after CO_2-treatment, progressing mass loss can be monitored after physical activation (table 1). Considering the constant 2 h annealing time, we see a correlation between the increase of the activation temperature and the mass loss, reaching a maximum value of −45 mass%

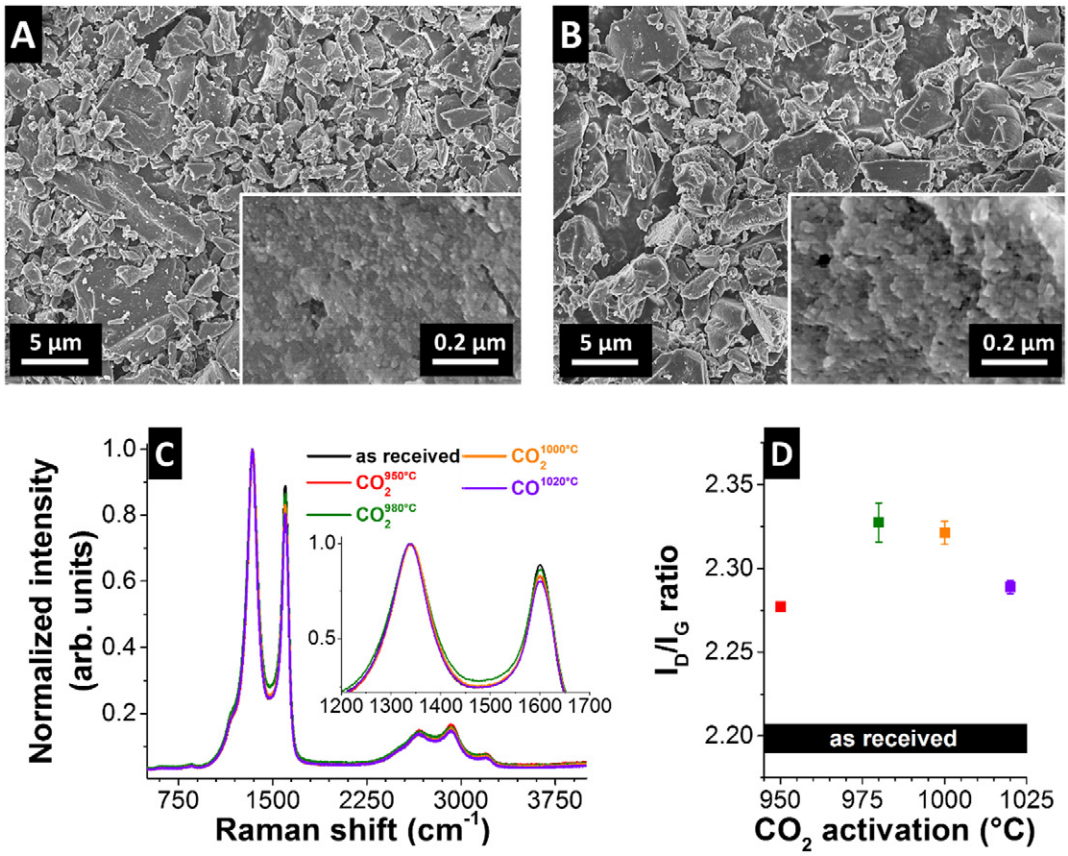

Figure 1. Scanning electron micrographs of activated carbon (A) as received and (B) after 2 h at 1020 °C CO_2-activation. (C) Raman spectra of as received carbon and carbons activated at different temperatures and (D) corresponding I_D/I_G ratio values.

Table 1. Porosity parameters derived from nitrogen gas sorption at −196 °C and corresponding mass losses (compared to as received) obtained from gravimetric analysis.

	Specific surface area ($m^2\ g^{-1}$)		Average pore size (nm)	Pore volume ($cm^3\ g^{-1}$)	Mass loss (mass%)
Temperature (°C)	BET	QSDFT	DFT	DFT	Gravimetry
as received	2107	1786	1.31	1.072	—
950	2261	1937	1.37	1.185	16
970	2314	2006	1.44	1.278	27
980	2329	2041	1.48	1.318	35
1000	2389	2121	1.56	1.426	37
1020	2363	2113	1.69	1.511	45

at 1020 °C. In parallel, we see a constant increase in pore volume and specific surface area (SSA), as shown in table 1 and figure 2. In comparison with as received powder, the QSDFT SSA can be increased up to 18% (i.e. +327 $m^2\ g^{-1}$) and the pore volume by +41% (i.e. +0.44 $cm^3\ g^{-1}$) after physical activation at 1020 °C for 2 h (as received: 1786 $m^2\ g^{-1}$ and 1.07 $cm^3\ g^{-1}$). As seen in table 1, the pore size distribution (figure 2(C)) shows an increase in total pore volume and an increase in average volume-weighted pore size from 1.31 nm to 1.69 nm. All nitrogen sorption isotherms belong to the type I with a small H4 hysteresis (figure 2(A)), indicative of predominantly microporous carbon with slit-shaped pores [44]. The correlation between activation temperature and average pore size or pore volume is highly linear ($R^2 = 0.9746/R^2 = 0.9979$) with a slope of 0.0045 nm/°C and 0.3623 $mm^3/g/°C$, respectively (figure 2(D)).

The activation process is not accompanied by significant changes in chemical composition. As confirmed by EDX, there is no statistically significant change in the total amount of oxygen in the samples: as received samples show a quantity of 1.9 ± 0.5 mass% oxygen, while activated material exhibits 1.7 ± 0.7 mass% oxygen.

More pronounced are the changes related to the wettability (figure 3(A)). When using film electrodes composed of as received material, we see a small initial contact angle of 63°. As expected for highly porous materials, the contact angle quickly decreases with increasing time due to capillary forces pulling the liquid inside the particle. This overall behavior is

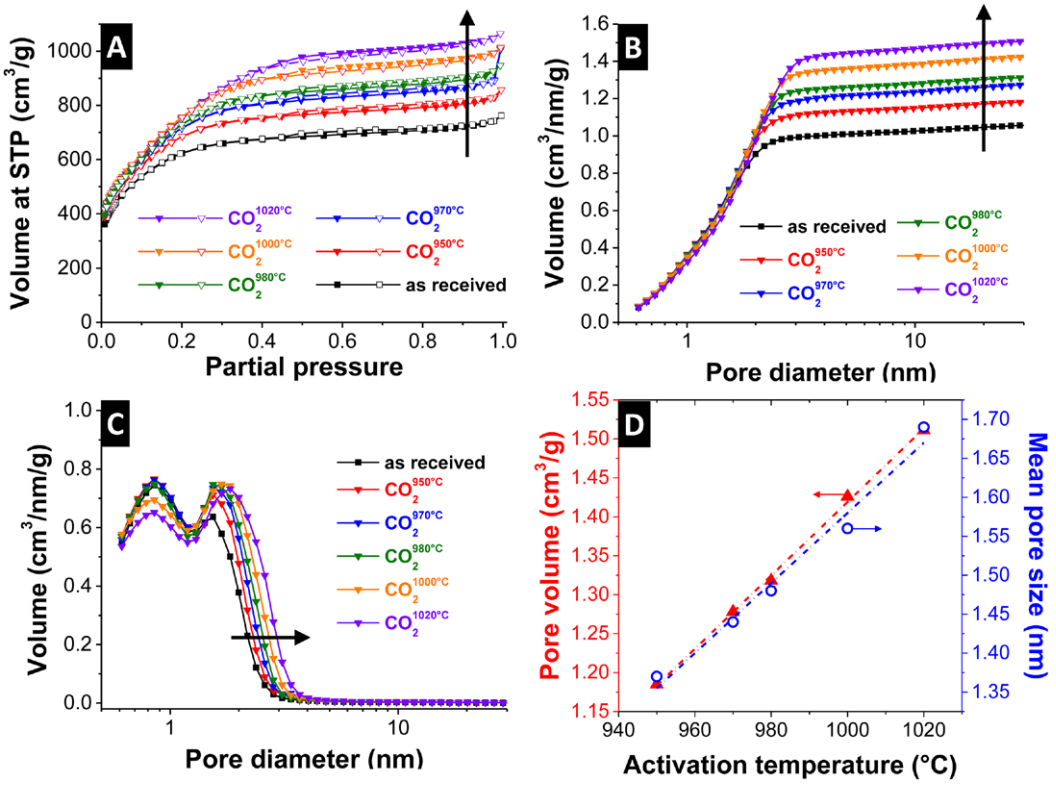

Figure 2. (A) Nitrogen gas sorption isotherms at standard temperature and pressure (STP), (B) QSDFT-derived corresponding cumulative pore size distribution, and (C) calculated differential pore size distribution pattern for different CO_2 activation conditions and as received. The arrows indicate the direction of increased activation temperature. (D) Average pore size and total pore volume as a function of CO_2 activation temperature.

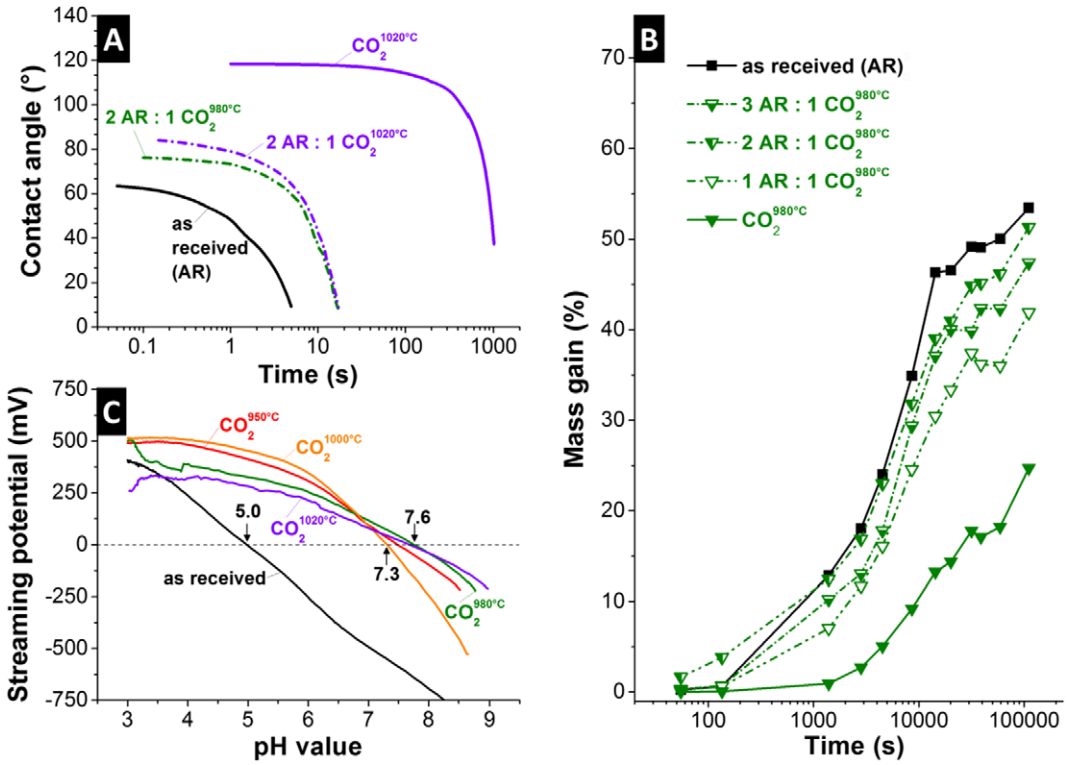

Figure 3. (A) Contact angle of film electrodes with water. (B) Water vapor uptake over time of film electrodes. (C) Streaming potential measurements of the activated material in comparison to as received.

maintained after CO_2-activation, for example at 1020 °C, but the initial contact angle becomes superhydrophobic (118°) and it takes more time to wet the sample. In particular, the as received material reach a contact angle of 20° after 4 s, but 1000 s for $CO_2^{1020\,°C}$. There was very little variation observed between samples activated at different temperatures. The initial contact angle decreased and the wetting process significantly improved when mixing as received powder with activated material, for example in a 2:1 ratio (2AR: 1 CO_2) with a start value of around 80° (figure 3(A)).

The changes in wettability are confirmed by a gravimetric study of the water vapor uptake as a function of exposure time to an environment constantly held at room temperature at 75% relative humidity (figure 3(B)). The as received material exhibits a more hydrophilic behavior, while the activated material, exemplified for $CO_2^{980°C}$, behaves the most hydrophobic. Intermediate states in the overall water uptake behavior can be adjusted gradually by admixing with the as received powder some activated material, as shown for 1:1, 2:1 and 3:1 mixing ratios (figure 3(B)).

The reason for this drastic change in the wetting behavior after CO_2-activation is related to a change of the surface termination of carbon. As shown by streaming potential measurements of the carbon powders (figure 3(C)), the as received material exhibits an isoelectric point at pH = 5.4 (obtained when using HCl as titrant and a starting pH of 9). This value is characteristic for carbons with predominantly carboxylic surface groups [29]. Decarboxylation as a result of the high temperatures applied during CO_2-activation can be seen by a strong increase in the pH position of the isoelectric point (iep) and all CO_2-treated samples show pH_{iep} values between 7.3 and 7.6 (almost independent of the activation temperature). This behavior is reasonable since at temperatures above 900 °C almost all of the oxygen containing acidic groups decompose and a back-formation under standard storage conditions is not possible [16, 26, 48]. The increasingly decarboxylated nature of the surface explains the more hydrophobic behavior after CO_2-activation [5, 27].

3.2. Electrochemical characterization in high molar saline water

We carried out CV and GC testing in 1 M NaCl aqueous solutions to provide a baseline for the electrochemical performance of the carbon materials. While this concentration is two orders of magnitude higher than what is later used for CDI, 1 M is a common concentration for aqueous supercapacitors. Also, the high ionic strength ensures mitigation of the diffusional and transport-related limitations of ion transfer occurring at low ion concentration and avoids counter-ion depletion. In addition, with the rising interest in aqueous supercapacitors [12, 17], our data using a high concentration of NaCl will be facile to adapt and transfer to the energy storage community.

Cyclic voltammetry (CV) at 10 mV s^{-1} shows the typical behavior of an electrical double-layer capacitor material for the samples before and after CO_2-activation, including a mixture of activated and as received carbon (figure 4(A)). In agreement with the wetting data, the capacitance decreases by ca. 9% when comparing the as received state with material activated at 980 °C which is also seen for other activation temperatures. Also, the resistive knee at the vertex potentials is more pronounced, which indicates a more resistive cell behavior. Yet, we note that the activated material has a much larger pore volume and surface area (e.g., $CO_2^{980\,°C}$: pore volume +23%, QSDFT SSA: +14%) and should, by this virtue, exhibit an improved capacitive performance. Interestingly, the resistive knee is more depressed and the capacitance is increased for a 2:1 mixture between as received material and, for example, CO_2^{980}. This mixture performs significantly better when compared to the activated material and even better in comparison to the as received material. CVs recorded at a low molar concentration typical for CDI (5 mM; figure 4(B)) display two important differences compared with data obtained at high molar concentration (figure 4(A)). First, the ion mobility is severely lowered and capacitive behavior is only seen at very low scan rates, as exemplified for 1 mV s^{-1} for as received material and after activation at 1020 °C in CO_2. As seen in figure 4(A), at high molarity (1 M), a highly capacitive behavior (i.e. rectangular CV) is already seen at a much higher scan rate of 10 mV s^{-1}. In addition, the CVs at 5 mM show at around 0.7 V cell voltage the emergence of ion depletion, as known for electrolytes with very low ion concentration [32, 55].

Additional insights into the performance as a function of current (power handling) can be gained by galvanostatic cycling to 1.2 V with different specific current (figure 4(C)). The as received material shows a specific capacitance of 134 F g^{-1} at a low current density of 0.1 A g^{-1}, dropping to 30 F g^{-1} at 8 A g^{-1}. In agreement with CV data and the wetting behavior, we see a severe drop in electrochemical performance after CO_2-activation, exemplified for $CO_2^{980\,°C}$ (106 F g^{-1} at 0.1 A g^{-1}). Mixing as received and activated materials is a facile method to significantly increase the capacitance and the best performance was encountered for a 2:1 mixture between as received and CO_2-treated carbon. In particular, we measured at 0.1 A g^{-1} for the 2:1 mixture a capacitance of 154 F g^{-1}, which is much higher than the 1:1 mixture (104 F g^{-1}) and the 3:1 mixture (126 F g^{-1}). We see in figure 4(C) that the capacitance for 2:1 mixture at low specific current is 14.9% and at high specific current more than 100% higher than for electrodes from as received powder. This increase of capacitance cannot be explained alone by SSA increase. The QSDFT SSA in film electrodes with 5 mass% PTFE was for AR 1625 m^2 g^{-1}, and for 2 AR + 1 $CO_2^{980\,°C}$ 1739 m^2 g^{-1}, which corresponds to a 7% SSA increase. In contrast, the increase of capacitance was more than 14%. Obviously, the interplay between improved wetting (as received material) and improved porosity data (CO_2-treated carbon) can be best exploited electrochemically when using a 2:1 mixture.

When comparing different activation temperatures (figure 4(D)), at low specific current, no systematic trend can be seen and all capacitance values scatter within a narrow margin (151 ± 3 F g^{-1}). We note that low specific current

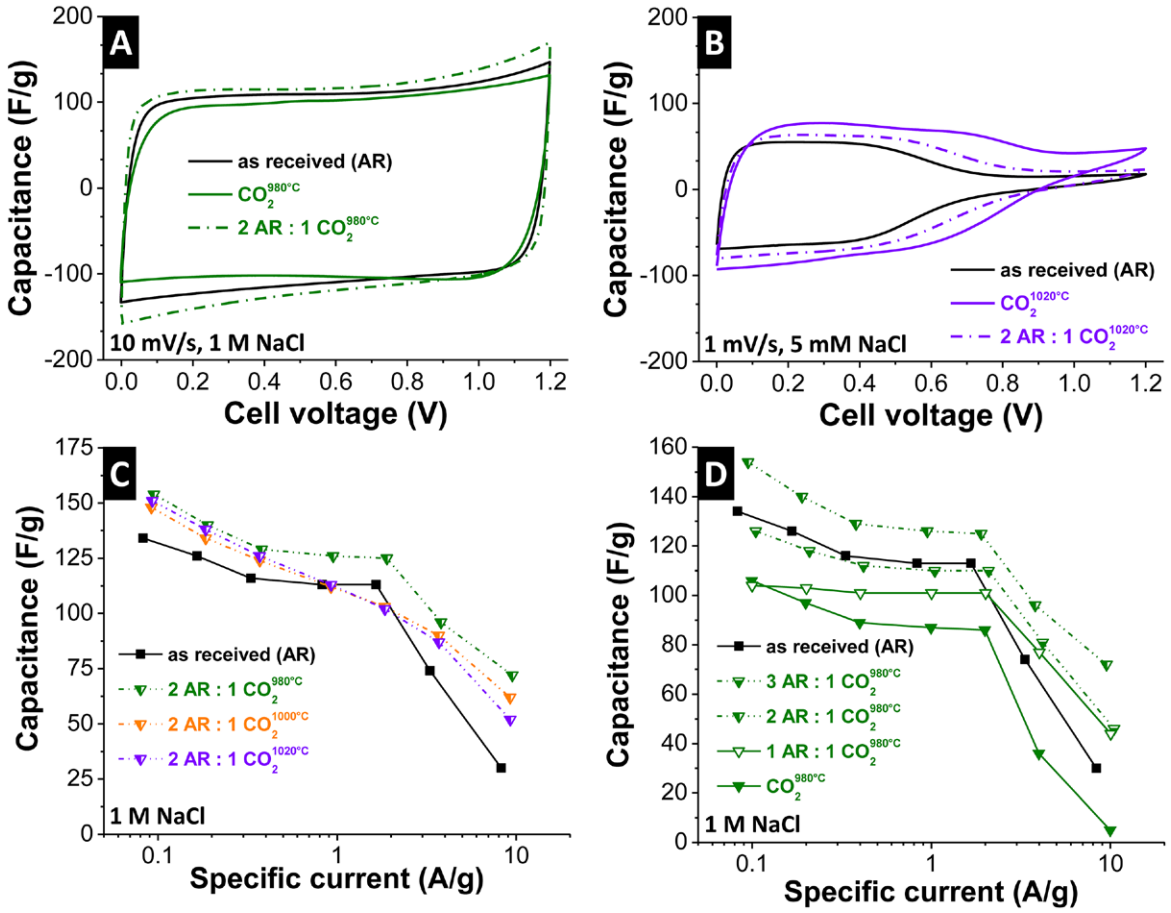

Figure 4. Electrochemical data. (A) Cyclic voltammograms at 10 mV s^{-1} in 1 M NaCl. (B) Cyclic voltammograms at 1 mV s^{-1} in 5 mM NaCl. (C), (D) Galvanostatic cycling to 1.2 V at various specific current values in 1 M NaCl.

values are most representative of the equilibrium capacitance. The latter is also more comparable to the CDI performance which is accomplished by charging and discharging for 30 min each. For comparison: a specific current of 0.1 A g^{-1} corresponds to a charging duration of ca. 20 min, while 10 mV s^{-1} (CV) corresponds to only ~2 min (figure 4(A)). Only at high specific current, when approaching 10 A g^{-1} we see a clear trend in favor of lower activation temperatures. In detail, the highest capacitance is encountered at 10 A g^{-1} for CO_2 $^{980\ °C}$ (72 F g^{-1}) followed by CO_2 $^{1000\ °C}$ (62 F g^{-1}) and CO_2 $^{1020\ °C}$ (52 F g^{-1}).

The electrode density also reflects the differences in pore volume. Using the same thickness of the film electrodes and 5 mass% of polymer binder, we obtain for the as received material 0.44 g cm^{-3} and 0.33 g cm^{-3} for CO_2 $^{1020\ °C}$. A 2:1 mixture of these two constituents yield 0.38 g cm^{-3}, which is close to the ideal mathematical average (0.39 g cm^{-3}). These values reflect the electrode density (mass loading/electrode volume), but not the skeletal density. According to the results of the helium pycnometer density measurements, the CO_2-treatment did not affect the skeletal density of AC powders (AR: $2.19 + 0.06$ g cm^{-3}, CO_2 $^{980\ °C}$: $2.11 + 0.01$ g cm^{-3}, CO_2 $^{1020\ °C}$: $2.18 + 0.03$ g cm^{-3}). Considering these results we can conclude that the lower density of electrodes containing CO_2-treated powder can be traced back to the higher specific pore volume in CO_2-activated AC powders.

3.3. CDI performance in low molar saline water

The CDI performance was characterized in batch mode using a saline concentration of 5 mM NaCl in demineralized water. If we were to use directly the specific capacitance from galvanostatic cycling at high molar concentration, and using a charge efficiency of 1, we would expect a SAC between 19 mg g^{-1} and 28 mg g^{-1}. This assumes a direct translation of each Coulomb of charge to the electrosorption of a corresponding counter-ion. Yet, such high values have not been reported for conventional CDI with AC so far, and excellent state-of-the-art AC materials exhibit values around 15 mg g^{-1} [34, 37]. Values up to 21 mg g^{-1} have recently been obtained from graphene-like foams exhibiting a very large pore volume of 3.13 cm^3 g^{-1} but very small surface area (<530 m^2 g^{-1}) [50, 51]. In alignment with our results, this indicates that pore volume instead of surface area should be the guiding parameter to select materials for high CDI performance.

Figure 5(A) depicts a typical charge/discharge (adsorption/desorption) cycle. To avoid skewing the data because of

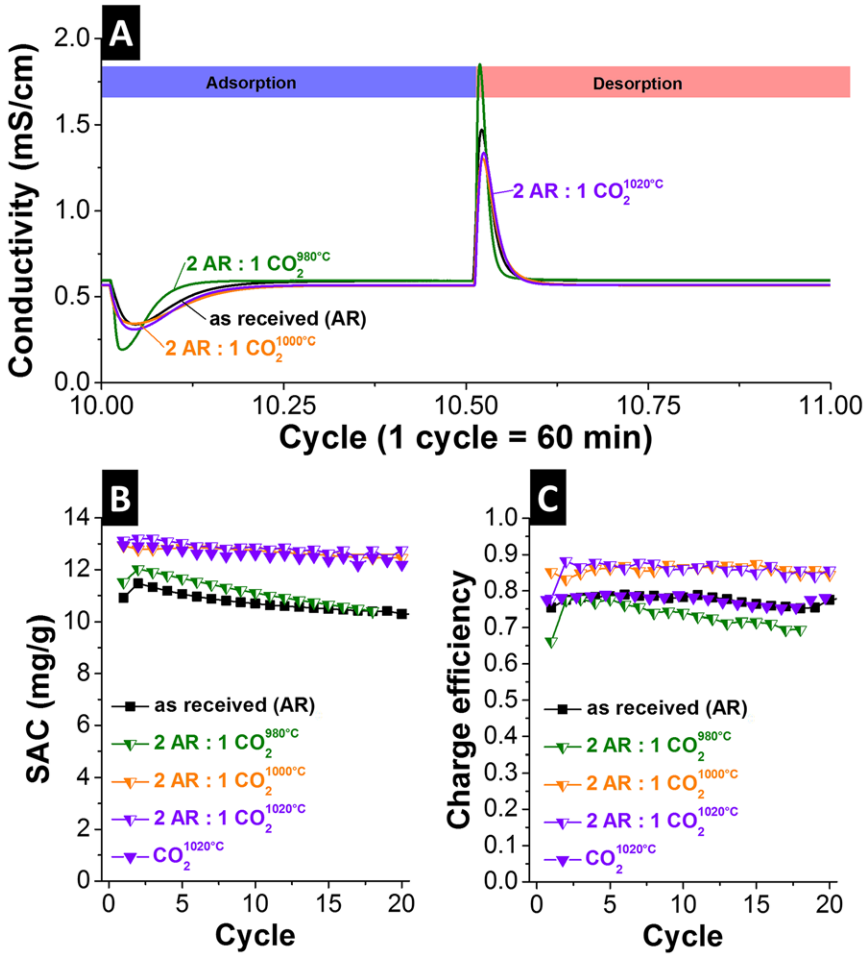

Figure 5. CDI performance in 5 mM NaCl at 1.2 V. (A) Conductivity data of the out-flowing stream for the 10th cycle. (B) SAC and (C) charge efficiency for 20 full cycles.

run-in effects during the first few cycles, we show here data of the 10th full cycle (each half-cycle takes 30 min). All film electrodes from each material exhibit the characteristic performance known from chronoamperometric (CAM) operation. During the ion-removal half-cycle, we see a significant decrease in the conductivity of the out-flowing stream, which declines over time as the electrodes reach their saturation. In contrast to the more gradual ion-removal, the desorption half-cycle (electrode regeneration) exhibits faster changes in out-flow conductivity, as common when discharging the system to 0 V. The fastest and strongest change in conductivity can be seen for a 2:1 mixture of as received material with CO_2 980 °C, while almost no difference is found between 2:1 mixtures using CO_2 1000 °C or CO_2 1020 °C. Yet, the latter two show larger areas when integrating the conductivity over time, which is indicative of a higher intrinsic SAC value.

The SAC performance, given in mg NaCl removed per g of carbon electrode, is shown in figure 5(B) with the corresponding charge efficiency depicted in figure 5(C). The charge efficiency will, for conventional CDI, always remain below 1 in reflectance of effects such as co-ion expulsion, specific adsorption or surface redox reactions, which do not contribute to the salt removal process but still consume a certain amount of electric charge. This consideration excludes non-conventional CDI approaches, such as inverted CDI (iCDI) [4, 20]. In our experiments, we chose 1.2 V cell voltage as a value high enough to ensure beneficial charge efficiency [54], but below the margin of the electrochemical stability window of water (at 1.23 V).

The CDI performance of as received material shows the lowest SAC values of all studied materials. After an initial increase from 10.9 mg g^{-1} to 11.5 mg g^{-1}, the CDI capacity decreases gradually and reaches 10.3 mg g^{-1} after 20 cycles. The charge efficiency remains rather constant at a low range of 0.75–0.79. These data align with reports of activated carbon CDI electrodes, where fluctuations during the first cycles have been studied as an effect of cell and electrode conditioning [10, 18].

In figures 5(B) and (C), we see a significant increase in SAC when employing 2:1 mixtures using as received material blended with CO_2 980 °C, CO_2 1000 °C and CO_2 1020 °C. 2:1 mixtures with CO_2 980 °C yield an initial SAC of 11.5 mg g^{-1}, but this value decreases gradually to 10.4 mg g^{-1} after 20 cycles. In parallel, the charge efficiency, starting at 0.66 and reaching a maximum at 0.77, also constantly declines to reach 0.69 after 18 cycles. A combination of improved SAC of ca. 13.1 mg g^{-1} with a very stable performance over 10 cycles (remaining at 0.86) is seen for the 2:1 mixtures using either CO_2 1000 °C or CO_2 1020 °C.

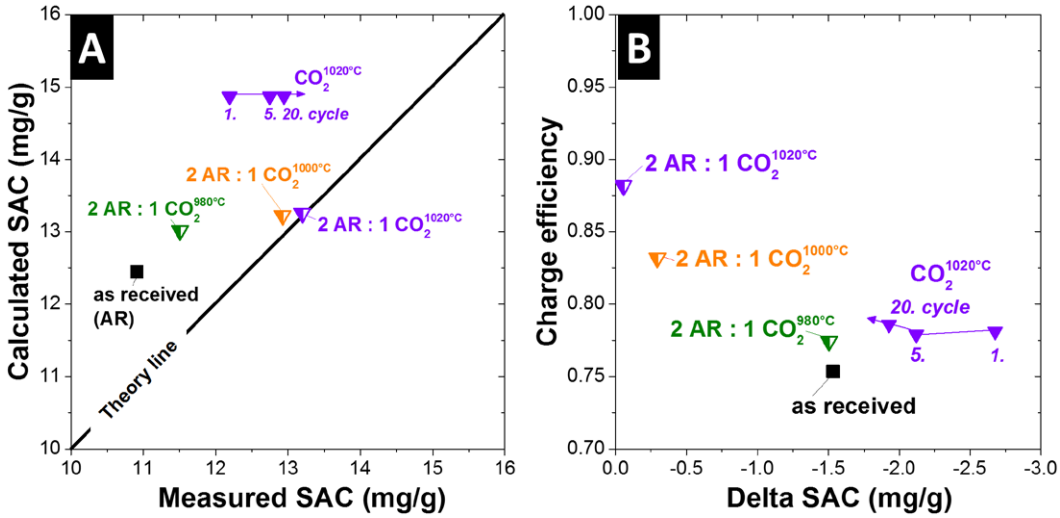

Figure 6. CDI performance in 5 mM NaCl at 1.2 V. (A) Parity plot comparing calculated and measured SAC values (calculated values based on the porosity data). (B) Comparison of the delta SAC (i.e., difference between calculated and measured SAC) plotted versus the measured charge efficiency.

Using the predictive SAC model introduced in [37], we can gain further insights into the behavior of as received and mixed carbon electrodes. This model is based on the cumulative pore volume, as measured by nitrogen gas sorption at −196 °C (see figure 2(B)). As shown in figure 6(A) for data of the first cycle, the as received material shows initially a deviation of 1.5 mg g^{-1} from the predicted value (10.9 mg g^{-1} instead of 12.4 mg g^{-1}). This deviation of 12% is understandable considering the low charge efficiency of 0.74. A correlation between deviation from the prediction and charge efficiency (delta SAC, as shown in figure 6(B)), aligns with recent results on heteroatom carbons with a large amount of electrochemically active surface groups [38]. As a general rule, a high charge efficiency translates to a higher accuracy of the predictive model. In our experiments, the best performance results were obtained for the 2:1 mixture with CO_2 $^{1020\ °C}$.

We also investigated the change in performance for film electrodes composed of only CO_2 $^{1020\ °C}$ material. We see that the charge efficiency remained rather constant from initially 0.78–0.79 after 20 cycles. The discrepancy between model and measurement (delta SAC) decreases from 2.7 mg g^{-1} to 1.9 mg g^{-1} after 20 cycles. The rather high deviation (even after 20 cycles) is reflective of the low overall charge efficiency. These data indicate that our model may assume a too large pore volume. Since we have seen a poor wetting behavior of pure or CO_2 $^{1020\ °C}$ (figure 3), it stands to reason to assume that not all of the available total pore volume actually participates in the ion electrosorption process. This is also in agreement with the increase in measured SAC cycle by cycle, while the charge efficiency remains on an almost constant high value.

4. Conclusions

We have provided a comprehensive study on the beneficial effect of CO_2-activation to tune and modify the pore structure of activated carbon. Significant increases in specific surface area and pore volume, at the expense of increasing average pore size, can be achieved by CO_2-activation at temperatures between 950 °C and 1020 °C. In particular, maximum values of 2113 m^2 g^{-1} (QSDFT SSA) and 1.51 cm^3 g^{-1} (pore volume) can be achieved with 2 h annealing in flowing CO_2 at 1020 °C. We also note that this improved porosity data is accompanied by a mass loss of up to 45%. This illustrates the challenges for balancing pore structure and burn-off when considering material and processing costs.

Another side-effect of the CO_2-treatment is the decarboxylation of the carbon surface, shifting the pH value of the isoelectric point from 5.4 to around 7.5. As a result, the material becomes more hydrophobic, making efficient wetting with water more difficult. A solution to this problem is presented by mixing as received powder (i.e., more hydrophilic) with CO_2-treated carbon (i.e., more hydrophobic). Our data show an improvement of the wetting behavior of the mixtures. Such a mixture, to the best of our knowledge, has not been proposed and explored in the literature so far for electrochemical applications in aqueous media.

At high molar concentration NaCl (1 M NaCl), we show a high specific capacitance of up to ca. 150 F g^{-1} for the mixtures. The best performance is encountered for a 2:1 mixture between as received and activated material. In comparison, the higher pore volume and surface area of the CO_2-treated material cannot be fully exploited by the electrolyte and the capacitance remains rather low (even lower than the as received material). The benefits of mixed hydrophobic/hydrophilic carbon electrodes are also available for CDI operations. A high and stable SAC of 13.1 mg g^{-1} with a charge efficiency of 0.86 is obtained for a 2:1 mixture of AR with CO_2 $^{1000\ °C}$ or CO_2 $^{1020\ °C}$.

In conclusion, our data show the facile application of CO_2-activation for CDI application enabling scalable material treatment (in our case: batches of 60 g) without the need for post-activation treatment (i.e., no washing, as required for KOH activation). Yet, because of the detriments to wetting, the improved pore structure can only be accessed by admixing

more hydrophilic carbon (in our case: as received material). In this way, high CDI performance in terms of SAC and charge efficiency can be obtained. This approach may also be applicable to aqueous supercapacitors, as indicated by our data in high molar concentration electrolyte.

We also note that these results align with the activities in the CDI community concerning adjusting surface chemistry of carbon electrodes. By finely adjusting the point of zero charge and the relative potential (and change thereof) of two electrodes, an electrode pair can be exploited to enhance the CDI performance significantly [4, 11, 30]. These effects can even be utilized in an inverse CDI process which holds the potential for improved long-term performance stability [19, 20].

Acknowledgments

We acknowledge funding from the German Federal Ministry for Economic Affairs and Energy (BMWi project no. KF2024309RH3) as part of the funding initiative 'Zentrales Innovationsprogramm Mittelstand' (ZIM). The authors thank Professor Eduard Arzt (INM) for his continuing support. We also thank our unnamed industry collaborator.

References

[1] Avraham E, Noked M, Cohen I, Soffer A and Aurbach D 2011 The dependence of the desalination performance in capacitive deionization processes on the electrodes PZC *J. Electrochem. Soc.* **158** P168–73

[2] Barbieri O, Hahn M, Herzog A and Kötz R 2005 Capacitance limits of high surface area activated carbons for double layer capacitors *Carbon* **43** 1303–10

[3] Biesheuvel P M 2009 Thermodynamic cycle analysis for capacitive deionization *J. Colloid Interface Sci.* **332** 258–64

[4] Biesheuvel P M, Suss M E and Hamelers H V M 2015 Theory of water desalination by porous electrodes with fixed chemical charge arxiv:1506.03948

[5] Brender P, Gadiou R, Rietsch J-C, Fioux P, Dentzer J, Ponche A and Vix-Guterl C 2012 Characterization of carbon surface chemistry by combined temperature programmed desorption with *in situ* x-ray photoelectron spectrometry and temperature programmed desorption with mass spectrometry analysis *Anal. Chem.* **84** 2147–53

[6] Brunauer S, Emmett P H and Teller E 1938 Adsorption of gases in multimolecular layers *J. Am. Chem. Soc.* **60** 309–19

[7] Centeno T A, Sereda O and Stoeckli F 2011 Capacitance in carbon pores of 0.7 to 15 nm: a regular pattern *Phys. Chem. Chem. Phys.* **13** 12403–6

[8] Chang L, Fu Z, Liu M, Yuan L, Wei J, He Y, Liu X and Wang C 2014 Optimal electrochemical performances of CO_2 activated carbon aerogels for supercapacitors *J. Wuhan Univ. Technol. Mater. Sci. Ed.* **29** 213–8

[9] Chmiola J, Yushin G, Gogotsi Y, Portet C, Simon P and Taberna P L 2006 Anomalous increase in carbon capacitance at pore sizes less than 1 nm *Science* **313** 1760–3

[10] Cohen I, Avraham E, Bouhadana Y, Soffer A and Aurbach D 2015 The effect of the flow-regime, reversal of polarization, and oxygen on the long term stability in capacitive de-ionization processes *Electrochim. Acta* **153** 106–14

[11] Cohen I, Avraham E, Noked M, Soffer A and Aurbach D 2011 Enhanced charge efficiency in capacitive deionization achieved by surface-treated electrodes and by means of a third electrode *J. Phys. Chem.* C **115** 19856–63

[12] Demarconnay L, Raymundo-Piñero E and Béguin F 2010 A symmetric carbon/carbon supercapacitor operating at 1.6V by using a neutral aqueous solution *Electrochem. Commun.* **12** 1275–8

[13] Dong Q, Wang G, Wu T, Peng S and Qiu J 2015 Enhancing capacitive deionization performance of electrospun activated carbon nanofibers by coupling with carbon nanotubes *J. Colloid Interface Sci.* **446** 373–8

[14] Farmer J 1994 Method and apparatus for capacitive deionization, electrochemical purification, and regeneration of electrodes. *US Patent* US5425858A.

[15] Ferrari A C 2007 Raman spectroscopy of graphene and graphite: disorder, electron–phonon coupling, doping and nonadiabatic effects *Solid State Commun.* **143** 47–57

[16] Figueiredo J L, Pereira M F R, Freitas M M A and Orfao J J M 1999 Modification of the surface chemistry of activated carbons *Carbon* **37** 1379–89

[17] Gao Q, Demarconnay L, Raymundo-Pinero E and Beguin F 2012 Exploring the large voltage range of carbon/carbon supercapacitors in aqueous lithium sulfate electrolyte *Energy Environ. Sci.* **5** 9611–7

[18] Gao X, Omosebi A, Landon J and Liu K 2014 Dependence of the capacitive deionization performance on potential of zero charge shifting of carbon xerogel electrodes during long-term operation *J. Electrochem. Soc.* **161** E159–66

[19] Gao X, Omosebi A, Landon J and Liu K 2015 Enhanced salt removal in an inverted capacitive deionization cell using amine modified microporous carbon cathodes *Environ. Sci. Technol.* **49** 10920–6

[20] Gao X, Omosebi A, Landon J and Liu K L 2015 Surface charge enhanced carbon electrodes for stable and efficient capacitive deionization using inverted adsorption − desorption behavior *Energy Environ. Sci.* **8** 897–909

[21] Gor G Y, Thommes M, Cychosz K A and Neimark A V 2012 Quenched solid density functional theory method for characterization of mesoporous carbons by nitrogen adsorption *Carbon* **50** 1583–90

[22] Hatzell K B, Iwama E, Ferris A, Daffos B, Urita K, Tzedakis T, Chauvet F, Taberna P L, Gogotsi Y and Simon P 2014 Capacitive deionization concept based on suspension electrodes without ion exchange membranes *Electrochem. Commun.* **43** 18–21

[23] Im J S, Kim J G and Lee Y-S 2014 Effects of pore structure on the high-performance capacitive deionization using chemically activated carbon nanofibers *J. Nanosci. Nanotechnol.* **14** 2268–73

[24] Jäckel N, Weingarth D, Zeiger M, Aslan M, Grobelsek I and Presser V 2014 Comparison of carbon onions and carbon blacks as conductive additives for carbon supercapacitors in organic electrolytes *J. Power Sources* **272** 1122–33

[25] Jeon S I, Park H R, Yeo J G, Yang S, Cho C H, Han M H and Kim D K 2013 Desalination via a new membrane capacitive deionization process utilizing flow-electrodes *Energy Environ. Sci.* **6** 1471–5

[26] Kundu S, Wang Y, Xia W and Muhler M 2008 Thermal stability and reducibility of oxygen-containing functional groups on multiwalled carbon nanotube surfaces: a quantitative high-resolution XPS and TPD/TPR study *J. Phys. Chem.* C **112** 16869–78

[27] Liu C, Liang X, Liu X, Wang Q, Teng N, Zhan L, Zhang R, Qiao W and Ling L 2008 Wettability modification of pitch-based spherical activated carbon by air oxidation and its effects on phenol adsorption *Appl. Surf. Sci.* **254** 2659–65

[28] Liu Y, Nie C Y, Liu X J, Xu X T, Sun Z and Pan L K 2015 Review on carbon-based composite materials for capacitive deionization *RSC Adv.* **5** 15205–25
[29] Marsh H 2006 *Activated Carbon* (Boston, MA: Elsevier)
[30] McCafferty E 2010 Relationship between the isoelectric point (pHpzc) and the potential of zero charge (Epzc) for passive metals *Electrochim. Acta* **55** 1630–7
[31] Mysyk R, Gao Q, Raymundo-Piñero E and Béguin F 2012 Microporous carbons finely-tuned by cyclic high-pressure low-temperature oxidation and their use in electrochemical capacitors *Carbon* **50** 3367–74
[32] Mysyk R, Raymundo-Piñero E and Béguin F 2009 Saturation of subnanometer pores in an electric double-layer capacitor *Electrochem. Commun.* **11** 554–6
[33] Noked M, Soffer A and Aurbach D 2011 The electrochemistry of activated carbonaceous materials: past, present, and future *J. Solid State Electrochem.* **15** 1563–78
[34] Omosebi A, Gao X, Landon J and Liu K 2014 Asymmetric electrode configuration for enhanced membrane capacitive deionization *ACS Appl. Mater. Interfaces* **6** 12640–9
[35] Oren Y and Soffer A 1978 Electrochemical parametric pumping *J. Electrochem. Soc.* **125** 869–75
[36] Pimenta M A, Dresselhaus G, Dresselhaus M S, Cancado L G, Jorio A and Saito R 2007 Studying disorder in graphite-based systems by Raman spectroscopy *Phys. Chem. Chem. Phys.* **9** 1276–90
[37] Porada S, Borchardt L O, Bryjak M, Atchison J S, Keesman K J, Kaskel S, Biesheuvel P M and Presser V 2013 Direct prediction of the desalination performance of porous carbon electrodes for capacitive deionization *Energy Environ. Sci.* **6** 3700–12
[38] Porada S, Schipper F, Aslan M, Antonietti M, Presser V and Fellinger T-P 2015 Capacitive deionization with novel biomass-based microporous salt templated heteroatom carbons *ChemSusChem* **8** 1867–74
[39] Porada S, Weinstein L, Dash R, van der Wal A, Bryjak M, Gogotsi Y and Biesheuvel P M 2012 Water desalination using capacitive deionization with microporous carbon electrodes *ACS Appl. Mater. Interfaces* **4** 1194–9
[40] Porada S, Zhao R, van der Wal A, Presser V and Biesheuvel P M 2013 Review on the science and technology of water desalination by capacitive deionization *Prog. Mater. Sci.* **58** 1388–442
[41] Raymundo-Piñero E, Cadek M and Béguin F 2009 Tuning carbon materials for supercapacitors by direct pyrolysis of seaweeds *Adv. Funct. Mater.* **19** 1032–9
[42] Raymundo-Piñero E, Kierzek K, Machnikowski J and Béguin F 2006 Relationship between the nanoporous texture of activated carbons and their capacitance properties in different electrolytes *Carbon* **44** 2498–507
[43] Simon P and Gogotsi Y 2008 Materials for electrochemical capacitors *Nat. Mater.* **7** 845–54
[44] Sing K S W, Everett D H, Haul R A V, Moscou L, Pierotti R A, Rouquerol J and Siemieniewska T 1985 Reporting physisorption data for gas/solid systems with special reference to the determination of surface area and porosity (Recommendations 1984) *Pure Appl. Chem.* **57** 603–19
[45] Stoller M D and Ruoff R S 2010 Best practice methods for determining an electrode material's performance for ultracapacitors *Energy Environ. Sci.* **3** 1294–301
[46] Suss M E, Baumann T F, Bourcier W L, Spadaccini C M, Rose K A, Santiago J G and Stadermann M 2012 Capacitive desalination with flow-through electrodes *Energy Environ. Sci.* **5** 9511–9
[47] Suss M E, Porada S, Sun X, Biesheuvel P M, Yoon J and Presser V 2015 Water desalination via capacitive deionization: what is it and what can we expect from it? *Energy Environ. Sci.* **8** 2296–319
[48] Szymański G S, Karpiński Z, Biniak S and Świątkowski A 2002 The effect of the gradual thermal decomposition of surface oxygen species on the chemical and catalytic properties of oxidized activated carbon *Carbon* **40** 2627–39
[49] Tuinstra F 1970 Raman spectrum of graphite *J. Chem. Phys.* **53** 1126
[50] Xu X, Pan L, Liu Y, Lu T, Sun Z and Chua D H C 2015 Facile synthesis of novel graphene sponge for high performance capacitive deionization *Sci. Rep.* **5** 8458
[51] Xu X, Sun Z, Chua D H C and Pan L 2015 Novel nitrogen doped graphene sponge with ultrahigh capacitive deionization performance *Sci. Rep.* **5** 11225
[52] Zhang R, Xu Y, Wen B, Sheng N and Fang H 2014 Enhanced permeation of a hydrophobic fluid through particles with hydrophobic and hydrophilic patterned surfaces *Sci. Rep.* **4** 5738
[53] Zhang S and Pan N 2015 Supercapacitors performance evaluation *Adv. Energy Mater.* **5** aenm.201401401
[54] Zhao R, Biesheuvel P M, Miedema H, Bruning H and van der Wal A 2009 Charge efficiency: a functional tool to probe the double-layer structure inside of porous electrodes and application in the modeling of capacitive deionization *J. Phys. Chem. Lett.* **1** 205–10
[55] Zheng J P and Jow T R 1997 The effect of salt concentration in electrolytes on the maximum energy storage for double layer capacitors *J. Electrochem. Soc.* **144** 2417–20
[56] Zickler G A, Smarsly B, Gierlinger N, Peterlik H and Paris O 2006 A reconsideration of the relationship between the crystallite size L_a of carbons determined by x-ray diffraction and Raman spectroscopy *Carbon* **44** 3239–46